SAE INTERNATIONAL

Computational Evaluation of Aerodynamic Forces on a Racing Motorcycle during High Speed Cornering

2015-01-0097
TSAE-15IC-0097
Published 03/30/2015

Tom Van Dijck
Oxford Brookes University

CITATION: Van Dijck, T., "Computational Evaluation of Aerodynamic Forces on a Racing Motorcycle during High Speed Cornering," SAE Technical Paper 2015-01-0097, 2015, doi:10.4271/2015-01-0097.

Abstract

This work describes the evaluation of the aerodynamic forces acting upon a road going sport motorcycle (modified for racing purposes) during a high speed, high lean angle cornering manoeuvre using commercial computational fluid dynamics software.

The subject of motorcycle cornering aerodynamics is currently one not widely covered in literature. The research presented in this paper aims to provide a basis for investigations into the improvement of motorcycle cornering performance through aerodynamic modifications.

Results were obtained through steady-state RANS simulation, using the k-epsilon turbulence model, of the vehicle during a cornering manoeuvre at a constant speed of 38 m/s with the lean angle varying from 45 to 55 degrees from vertical. This manoeuvre was analysed in 1 degree intervals.

Large lift forces were observed, with centre of pressure located near the front of the motorcycle, which increase as the motorcycle leans further. The effect of drag on yaw and pitch moment, due to the motorcycle's orientation, was found to be substantial compared to aerodynamic side-forces developed. Modifications of windscreen and bellypan are presented to show methods of influencing the magnitude of developed lift and side-force.

Introduction

The subject of motorcycle cornering aerodynamics has previously been brought up by various authors. (Foale, 2004) discusses past attempts at improving motorcycle cornering performance through the addition of wings. Though this may have been a viable option in days when motorcycle lean angles were modest, today's Grand Prix motorcycles will reach up to 64° of lean. Using rigidly fixed wings during such a cornering manoeuvre would result in a side-force, pushing the motorcycle out of the corner, far greater than the additional downforce loading the tyre contact patch. Indeed, equation 1 shows the tyres' friction coefficient would have to be over 1.73 for the wings to provide any additional cornering performance at all.

$$\frac{atera}{vertical} = \frac{wing \sin(64°)}{wing \cos(64°)} = 1.73 \quad (1)$$

A tilting wing (Fig. 1), held horizontal through use of gyroscopes, would provide a solution to this issue. Such active aerodynamic appendages are however illegal in all major racing series, the most likely development ground for such performance improving technologies.

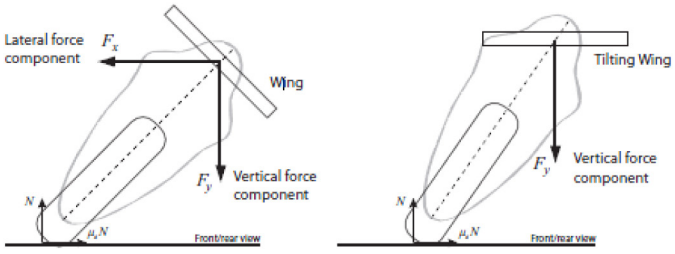

Figure 1. Motorcycle wing configurations, depicting limitations of fixed wing (left) and advantage of gyroscopically balanced wing (right). [8]

A different approach, utilising rider interference, was investigated numerically by (Sedlak, 2012). Winglets are mounted on either side of the motorcycle, angled so that the winglet on the outside of the corner is positioned horizontally when the motorcycle is at maximum lean angle. The inside winglet's efficiency at generating harmful sideforces is reduced due to the rider hanging off the motorcycle interfering with the flow aft of the winglet.

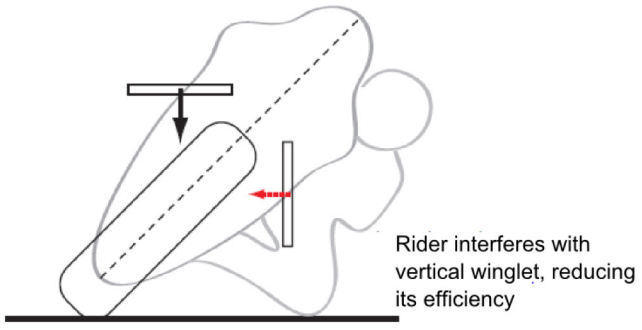

Figure 2. Motorcycle winglet concept [8].

Sedlak's research focuses mainly on the viability of using the rider-wing interference effects to stall the in-corner winglet, though a preliminary full-scale 3D simulations shows promising results in terms of high downforce to sideforce ratios.

Other research on the subject of improving motorcycle cornering performance through aerodynamics is not readily available in literature. There are however many indications that teams in the highest racing classes have managed to use the flow of air around their machines to their advantage.

(Foale, 2004) reports on Reynard Motorsports Ltd. having done research into shaping the underside of the bellypan fairing to develop a side-force, adding directly to the tyre forces sustaining cornering. Their results are however not openly available.

Similarly, in the presentation of their 2006 M1 MotoGP machine, Yamaha Factory Racing discusses how they sacrificed some of the vehicle's straight-line aerodynamic performance for an improved side yaw characteristic, which was said to improve the vehicle's agility. A full explanation of what was meant by this side yaw characteristic or in what ways it improved agility is however not available.

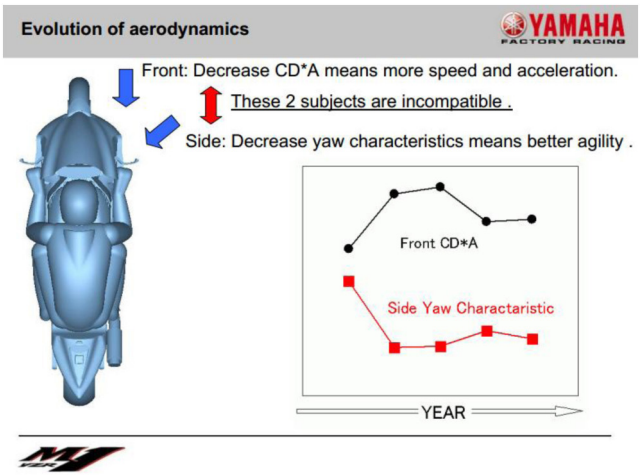

Figure 3. Evolution of aerodynamics for the YZR-M1 [12]

It appears then, that aerodynamics can be used to improve a motorcycle's cornering performance and/or stability. There is though a lack of data in published literature, making it difficult to decide on the right approach to take. It is the aim of this paper to provide a basis to those wishing to start research into improving motorcycle cornering aerodynamics.

In the following chapter, a full description of the simulation model will be given, including the mesh and solvers used and a full description of the boundary conditions applied. The results of the simulations will then be discussed in the next chapter, first looking at a straight-line acceleration scenario for comparison purposes, then discussing the magnitude and effect of each orthogonal force (drag, lift, side-force) and the moments individually. A modified geometry and its effect on aerodynamic forces is then discussed, followed by a concluding chapter.

2. Methodology

2.1. Geometry

The work described in this paper was, simultaneously with a straight-line drag optimisation, carried out for a team currently racing in the British SuperBike series. As such, the subject of the investigations is the motorcycle they currently race: a 2013 Kawasaki ZX10-R in SuperStock racing trim (e.g. rear-view mirrors and license plate removed, bellypan added …). Exterior body geometry was modeled with high accuracy, but components with no outright aerodynamic function were simplified (i.e. engine, brake discs, wheels …).

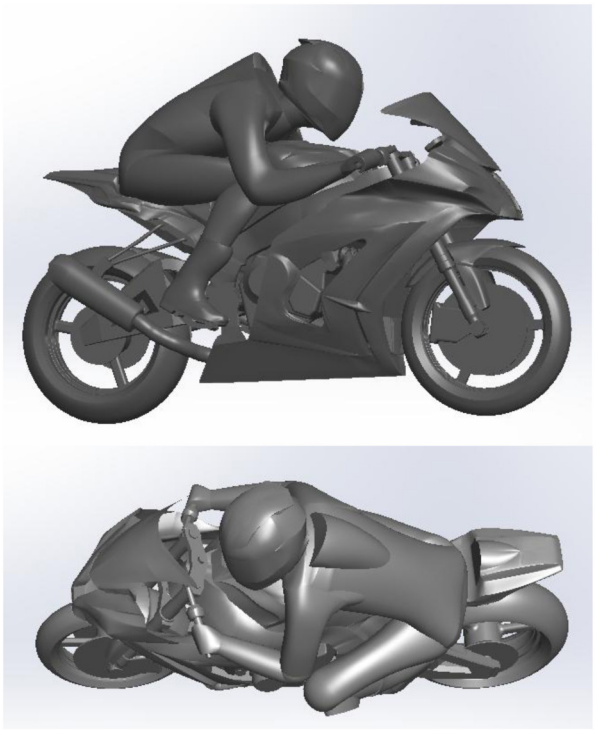

Figure 4. Motorcycle and rider CAD geometry for straight-line acceleration (Top) and high speed cornering (Bottom).

The rider's influence on the motorcycle's aerodynamics has been previously demonstrated (>19% of frontal area even in the prone straight-line position [9]). For the simulations, the previously mentioned team's experienced professional rider's body positions were modeled for straight-line acceleration (for use in the benchmarking test) and high speed cornering cases. Though in reality the rider's body position during cornering is dynamic, a single representation was used for all simulations.

2.2. Physics Models

Results were obtained through computation of the steady-state Reynolds Averaged Navier-Stokes (RANS) equations for incompressible flow. Though bluff body (motorcycle) aerodynamics are inherently unsteady, a steady solver (as used in this work) requires far less resources and can provide accurate results in terms of absolute values and trend prediction [2][10]. The Realizable Two-layer k-ε model was chosen, to provide closure to the RANS equations, for its robustness, low resource requirements and because it has been previously shown to provide good accuracy in motorcycle straight-line simulation [11][5].

2.3. Boundary Conditions

The simulation speed was set at 38 m/s (85mph) for a Reynolds number of 4.92×10^6 (Reference length = 2.1m). This was deemed to be a high cornering speed, where aerodynamic forces play the largest role, after analysis of British SuperBike performance on various UK circuits.

The range of roll angles to be investigated was also set during this analysis. The maximum roll angle achieved during cornering at this speed is roughly 55 degrees from vertical, which was set as the upper limit in the simulations. 45 degrees from vertical was arbitrarily set as the starting point. The transition from 45° to 55° was simulated in steps of 1°.

A motorcycle almost never corners at constant lean angle for long and so experiences a certain magnitude of roll rate. For the range of lean angles considered during this investigation, the roll rate generally ranges from 0 to 0.25rad/s. Simulations incorporating this roll rate were run, but the effect on aerodynamic forces and pressure distributions was deemed insignificant at <1.5%.

Wheel rotation and moving floor were set to match the simulation speed. Turbulence intensity and length scale were set to 3% and 3m respectively, as this has been shown to give better approximation of open road conditions [6].

2.4. Radiator Modeling

Radiators are often omitted from full vehicle CFD studies, unless under-hood or cooling flows are part of the problem definition. Racing motorcycles however, with their high power density engines, require comparatively large and efficient radiators, which contribute greatly to drag (over 12.7% of overall drag in this study, radiator shape- and cooling drag combined). The difference between modeling the radiator as a solid, non-permeable block and as its actual porous state can amount to a 6% difference in total vehicle drag, as demonstrated experimentally by (Scappatici et al., 2012) and verified numerically by the author.

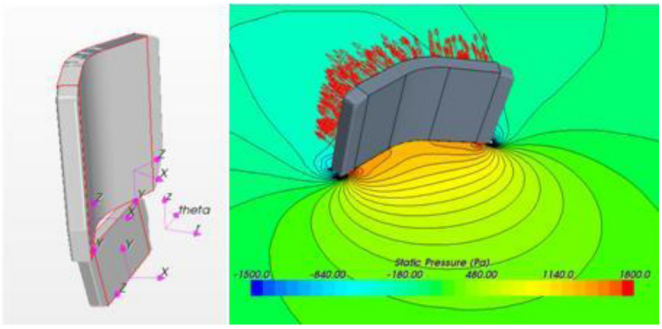

Figure 5. Simple radiator volumes (Left) and Porous radiator model with pressure drop and flow straightening visualised (Right).

Using detailed geometry of a radiator, with its thousands of cooling fins, comes at great computational expense. For this reason, porous models of the ZX10-R's radiator and the supplementary KX450F dirt-bike oil cooler were implemented into the simulations. The radiators are represented by simple volumetric geometry with the correct dimensions (Fig 5). A pressure drop model is then introduced for flow that passes through this geometry. The pressure drop the flow experiences in the direction it normally passes through the radiators(for the curved radiator section, this was the radial direction of a cylindrical coordinate system) is defined by Eq. 2. The other two orthogonal directions are assigned much higher (x1000) values of resistance to completely restrict fluid flow and thus model the flow straightening effect of the radiator.

$$\frac{\Delta P}{l} = -[P_i u^2 + P_v u] \tag{2}$$

With ΔP/l the pressure drop per unit length, P_i the coefficient of inertial resistance and P_v the coefficient of viscous resistance.

The aforementioned resistance coefficients are commonly determined experimentally running wind tunnel tests of the radiator at varied inlet speeds (e.g. [4]). When appropriate facilities are unavailable, CFD can provide an alternative however. An approach similar to that taken by (Bella et al., 2013) was followed.

Figure 6. Detailed radiator geometry partition.

Radiator geometry with accurate fin dimensions and fin density, though simplified fin shape, was created. A small section of this geometry was submitted for CFD simulation at various inlet speeds and the pressure drop across the radiator was measured. A 2nd order polynomial fitted to the results gives the resistance coefficients. This was done separately for the radiator and oil cooler. As can be expected, the dense, high efficiency racing water radiator has much higher resistance than the rugged oil cooler which was designed for a low power density dirt bike.

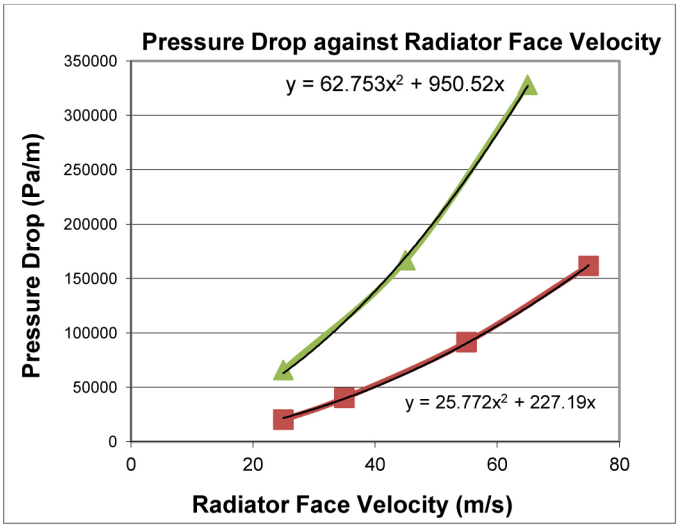

Figure 7. Pressure drops across KX450F oil cooler (Red) and ZX10-R radiator (Green).

2.4. Computational Domain

Incorporating the yaw motion a vehicle performs during cornering into aerodynamic experiments would require the use of a curved wind tunnel with curved flow. This is currently not feasible in even the latest wind tunnels, however numerical simulation is not limited in this way. In the software used, STAR-CCM+, the inlet flow can simply be defined along the tangential axis of a cylindrical coordinate system set at the centre point of the vehicle's cornering path. The fluid domain should be curved to match the resulting flow curvature.

Figure 8. Flow curvature definition in Star-CCM+ using cylindrical coordinate system.

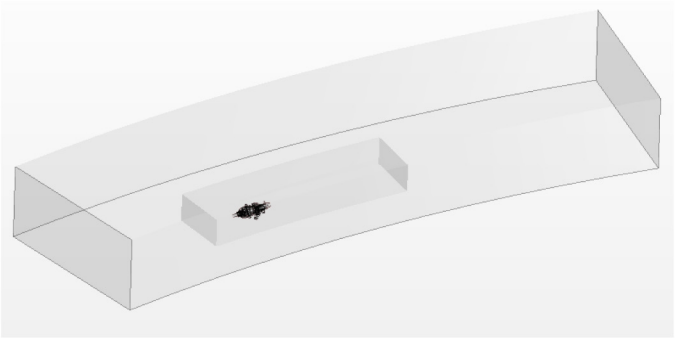

Figure 9. Computational domain for motorcycle cornering simulations. (Coarse mesh refinement region also pictured)

The simulation speed was set as a constant to maintain Reynolds number (Re=4.92 × 10^6). The corner radius R required to create the correct fluid domain and inlet conditions was then calculated for every lean angle φ investigated:

$$R = \frac{u_{in}^2}{\tan(\varphi) g} \quad (3)$$

With u_{in} the inlet speed and g the gravitational constant.

The fluid domain thus had a radius ranging from 132m at 45° (note: 3° was added to the motorcycle lean angle to account for the effect of the rider hanging off) to 92m at 55° of lean. It was dimensioned to simulate open road conditions (Table 1), i.e. large enough not to affect simulation results. Side walls and ceiling were defined as slip-walls.

Table 1. Computational Domain Dimensions.

Length	5 Vehicle lengths fore, 10 vehicle lengths aft
Width	13 Vehicle widths
Height	5 Vehicle heights
Blockage Ratio	1.5%

2.5. Mesh

Meshing was performed in STAR-CCM+, using the polyhedral mesher tool. The mesh size was allowed to grow to 2000% of the assigned base value from the coarse refinement region (Fig. 9)(400%) to the outer walls of the fluid domain. Additional refinement was defined in the vehicle and vehicle wake region (from vehicle leading edge to 1 vehicle length behind, set at 100% base value) and wheel and radiator wake regions (50% base value). A base value of 23.5mm was found to be sufficient to guarantee grid independency of results.

Prism-type cells were used for modelling of the near-wall flow. Similar to the method followed by (Shimizu et al., 2009), boundary layer resolution (y+ < ~1) was employed on key aerodynamic components (front wheel assembly, windscreen, main fairing, rider …), using up to 12 prism layers. For other components (engine …) wall laws were used to model the boundary layer (30 < y+ < 350).

The final mesh consisted of 12 million cells, resulting in simulation times of 14 hours/run on a high-end desktop computer with 3.4GHz octocore processor.

3. Results

3.1. Straight-Line Benchmark

A simulation of the vehicle-rider combination during straight-line acceleration at 38 m/s was run as a reference point for comparison with the cornering simulation data. Lift and drag force coefficient results are displayed in Table 2.

Table 2. Results: Straight-line acceleration with rider prone.

Frontal Area A [m²]	0.5924
Coefficient of Drag C_D	0.536
Drag Area C_DA [m²]	0.318
Centre of Pressure Height [m]	0.65
Coefficient of Lift C_L (Total)	0.009
Coefficient of Lift C_{Lf} (Front Wheel)	-0.053
Coefficient of Lift C_{Lr} (Front Wheel)	0.062

An insignificant amount of sideforce was also present due to slight lateral asymmetry (exhaust location, bodywork shaped around asymmetric engine …).

The results of this benchmark simulation can be compared to those gathered by (Schütz, 2013) through experimental analysis of the BMW S1000RR (A=0.60 m², C_D=0.52)(rider included), which has a high level of similarity to the ZX10-R and races in the same superbike classes.

3.2. Cornering Simulations

This chapter discusses the results of the simulations of the high speed, high lean angle manoeuvre. The three orthogonal aerodynamic forces (drag, lift, side-force) are discussed separately, followed by a discussion of their combined effect on tyre contact patch loads and the motorcycle's rolling moment. Note that the frontal area is the reference area A used in all coefficient calculations:

$$C_x = \frac{F_x}{\frac{1}{2}\rho V^2 A} \quad (4)$$

3.2.1. Drag

The pose a rider assumes during cornering in order to reduce the motorcycle's lean angle and control wheel loads has him hanging a large part of his body outside the extremities of his motorcycle. This results in an increase in frontal area of 38.7% (from 0.59 to 0.72m^2). This is accompanied by an increase in drag coefficient due to the aerodynamic inefficiency of this body position, with large areas of flow stagnation on the rider's helmet, arms and inside leg.

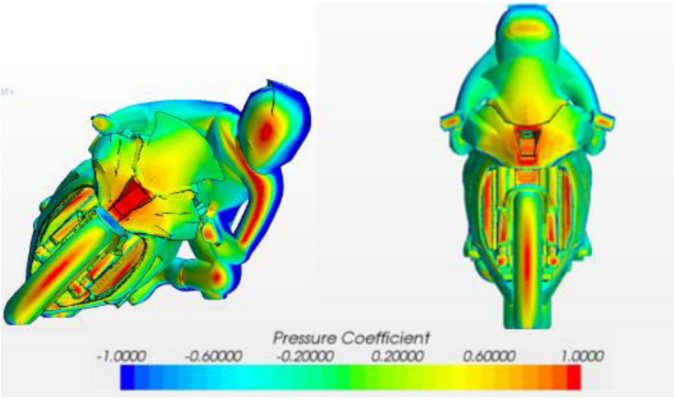

Figure 10. Pressure coefficient distribution on frontal plane of motorcycle-rider combination.

The rider's more upright body position also results in a much earlier onset of flow separation on the rider's back.

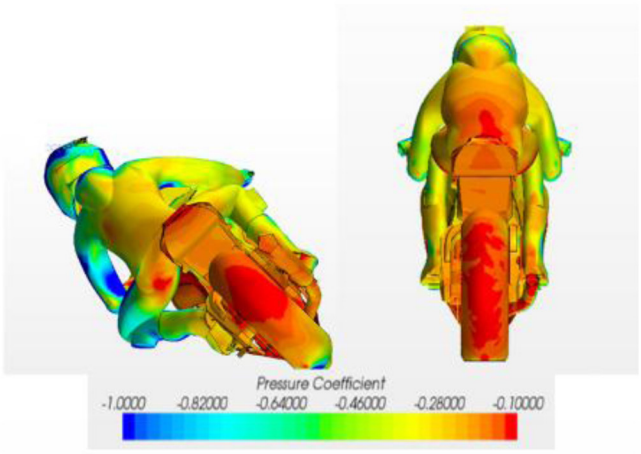

Figure 11. Pressure distribution on rear view of motorcycle rider combination.

The combination of these two effects result in an increase of the drag coefficient from 0.536 in the straight-line case to 0.58 at 45° of lean, further increasing near-linearly to 0.61 at 55°. Note Fig. 12 shows a drop-off in drag area at the highest lean angles. This is due to a small intersection of the rider's knee with the computational domain's floor causing decreased frontal area. In a realistic scenario, the rider would retract his knee inward as it makes contact with the ground.

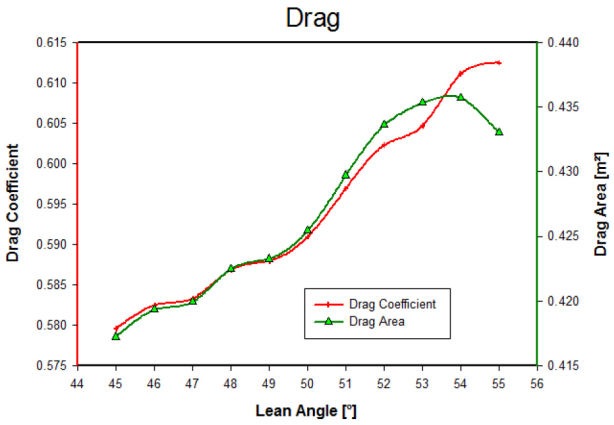

Figure 12. Drag Coefficient and Drag Area variation with lean angle.

Due to the motorcycle's orientation in roll, the centre of pressure (CoP) for drag is lowered, reducing the pitching moment that causes unloading of the front wheel, but it is also displaced laterally from the tyre contact patch plane. This results in a yawing moment which turns the vehicle into the corner, and which increases with lean angle. The effect on wheel loads is shown in Fig. 14. Note a negative coefficient of side-force denotes a side-force pointing into the corner, thus aiding cornering.

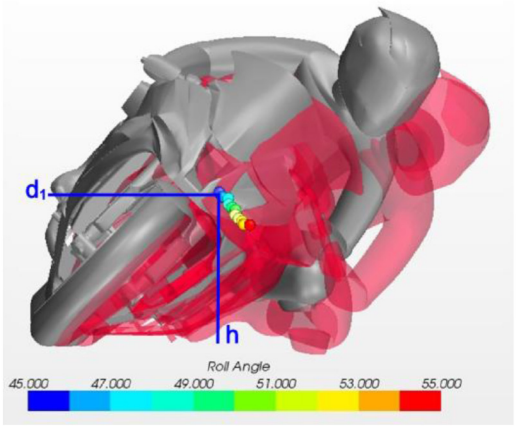

Figure 5. CoP for drag position with varying roll angle (Front view).

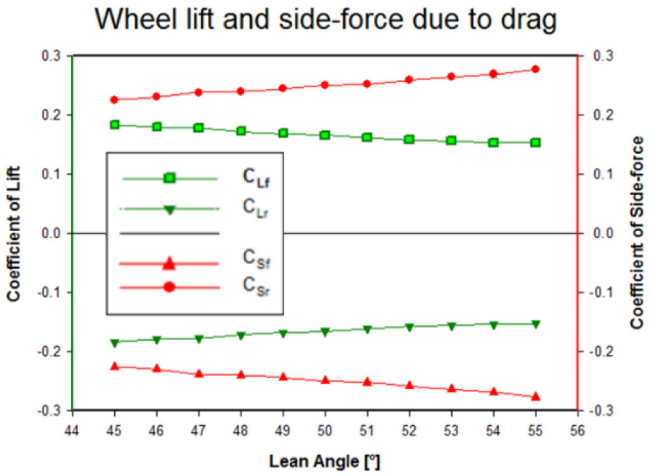

Figure 14. Effect of drag on wheel loads.

3.2.2. Lift

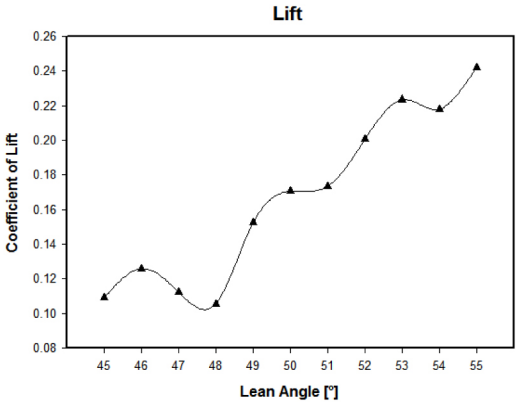

Figure 15. Lift-lean angle relation.

As the motorcycle rolls the gap between the ground and the side of the motorcycle decreases, while the flow through this gap is obstructed by the rider's body. An increase in lift coefficient from 0.009 at 0° roll to 0.109 at 45° was observed after the first simulation. The initial jump in lift can be attributed to the smooth high speed flow over the top-facing side of the motorcycle as well as the rider's body (which attributed 15-20% of total lift) (Fig 16).

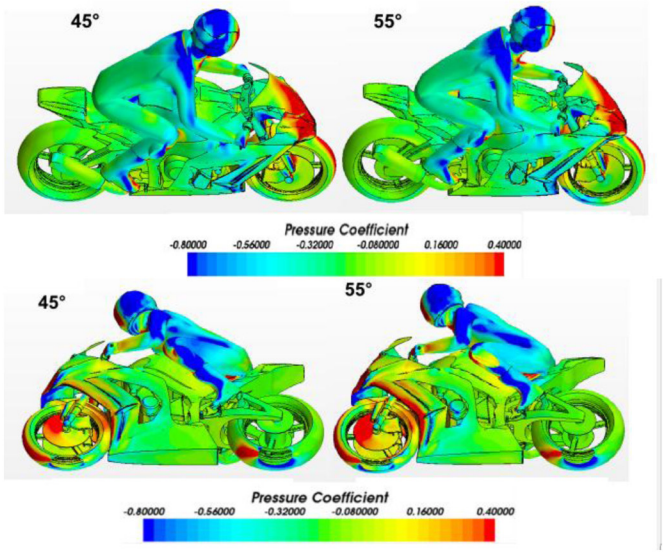

Figure 16. Pressure distribution on motorcycle-rider surfaces in top view (top) and bottom view (bottom).

As the motorcycle leans further, the high pressure region pushed in front of the vehicle interacts with the ground and propagates rearward. The resulting high pressure field in the gap between the front of the motorcycle and the ground causes a substantially increase in lift coefficient to a maximum of 0.267 at 55°.

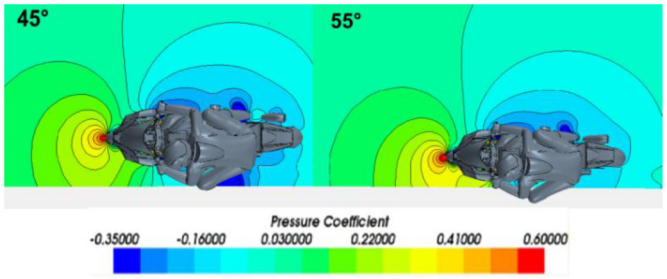

Figure 17. Vehicle-Ground interaction (Top view, vehicle fixed coordinate system).

The effect described above also results in a forward placed centre of pressure, which displaces forward with increasing lean angle. The result is a rear wheel lift force which remains relatively low, but a front wheel lift which increases significantly (+190%), to a value 3x the rear lift, as the vehicle leans from 45° to 55°.

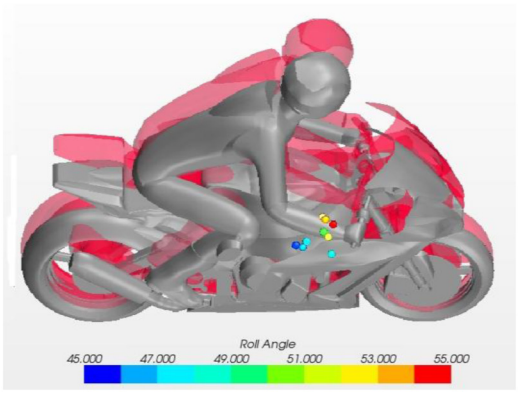

Figure 18. CoP of lift displacement with roll angle (Top view).

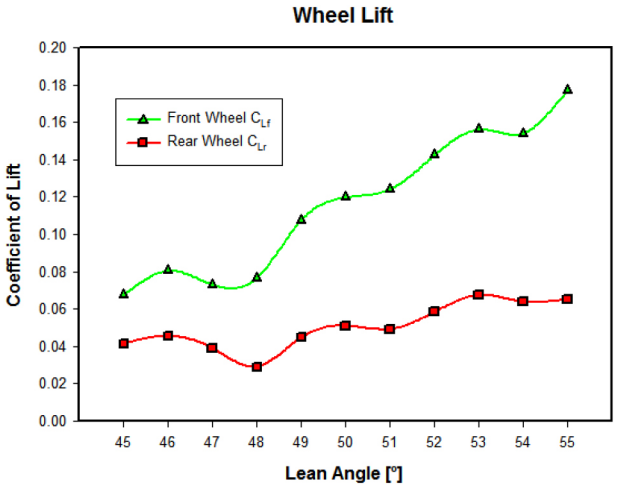

Figure 19. Wheel lift variation.

3.2.3. Side-Force

The relationship between lean angle and side-force does not vary as linearly as that of the other two orthogonal forces. It's effect on the forces acting at the tyre contact patches is consistent however, in that the vehicle always experiences a yaw moment that turns the vehicle out of the corner, e.g. understeer.

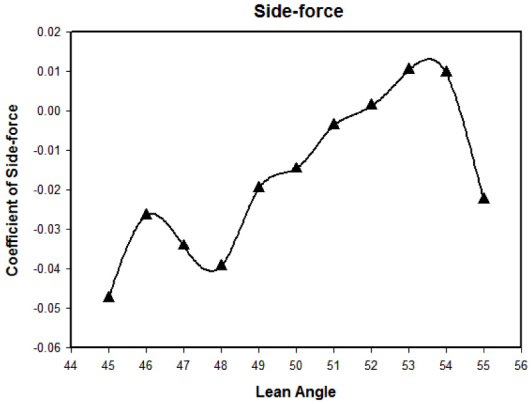

Figure 20. Side-force variation.

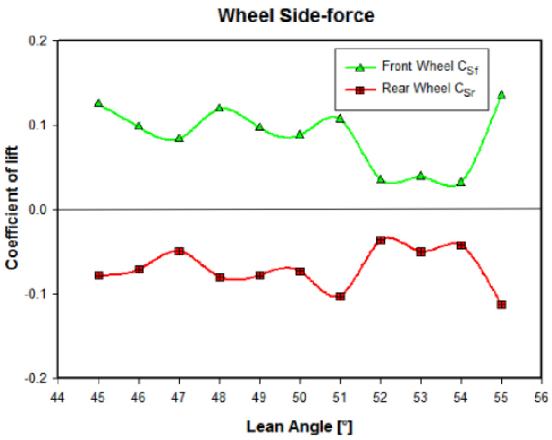

Figure 21. Wheel side-force variation.

The same high pressure field propagation into the wedge between motorcycle and ground that causes the increase in lift also explains the front wheel side-force. The orientation of the windscreen also causes a net force pushing the front wheel out of the corner. The rear wheel negative side-force is largely caused by the low pressure regions resulting from the high flow acceleration around the rider's body. The combination of these effects causes a high yawing moment, explaining the position of the CoP, which lies far outside the vehicle's boundaries.

Figure 22. CoP for sideforce displacement with roll angle (Right view).

The radiators contribute greatly (>25%) to side-force as well, increasing linearly with lean angle. While the air flow separates and is guided away from the radiator entrance on the right side (outside of corner) of the motorcycle, the high pressure region on left side promotes attachment and increases airflow towards the inside side of the radiator. Due to its angled orientation, it produces a net side-force into the corner.

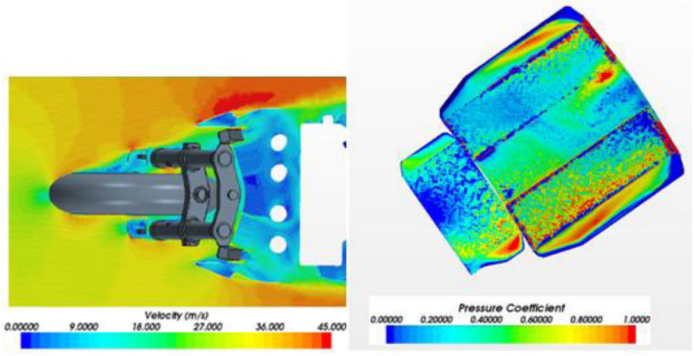

Figure 23. Flow velocity (left) Pressure distribution on radiator (right) for 55° lean.

3.2.4. Combined Wheel Loads

The previous sections covered each of the 3 orthogonal aerodynamic forces' causes and effects individually. This chapter shows the compound effects on front and rear wheel loads.

The decrease in pitching moment due to drag cannot offset the sharp increase in front lift force, resulting in a linearly decreasing front wheel load. On the other hand, the decrease in pitching moment is the dominant factor for the rear wheel load, resulting in a steady decrease of the downforce acting on it.

The oversteering yawing moment caused by drag is large enough to offset the understeering effect of the generated side-forces, resulting in an overall oversteering effect, which is a dynamically stable condition for single-track vehicles.

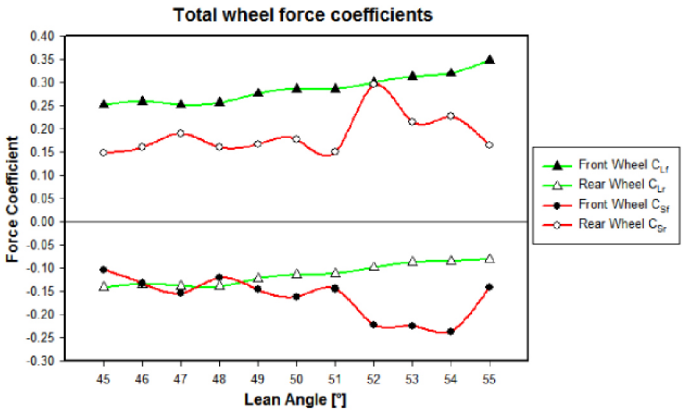

Figure 24. Compound effect of aerodynamic forces on wheel loads.

3.2.5. Rolling Moment

Side-forces and primarily the lift force result in a moment around the vehicle's roll axis. This moment attempts to right the motorcycle, an effect which increases with roll angle.

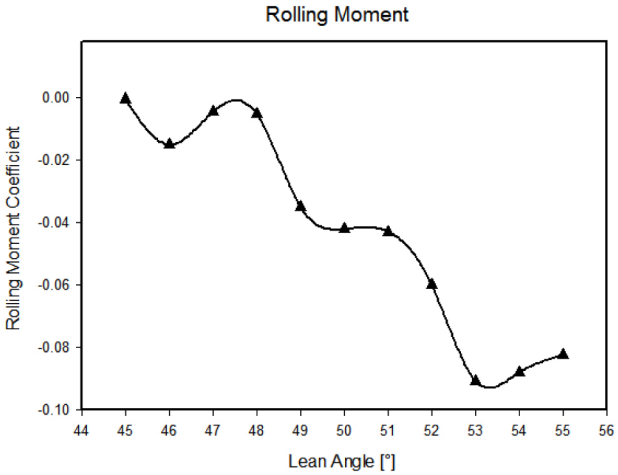

Figure 25. Rolling moment- Lean angle relation.

3.3. Modifications

A modified version, optimized for minimum straight-line drag within MCE British SuperBike regulations, was simulated at a lean angle of 55° to assess the effect of the modifications on cornering performance. (See Appendix A for modifications)

This drag-optimised shape investigated also reduces the total lift force under maximum lean by 10%. Combined with the reduction in drag of 5.8% (diminished from straight-line case's 12.8% due to an ineffective windscreen in lean) reducing the pitching moment, this results in a reduction of front wheel lift of 25%.

Table 3. Comparison of stock and modified motorcycles.

	SuperStock	SuperBike (modified)
Frontal Area	0.707	0.721
C_DA [m²]	0.433	0.408
C_LA [m²]	0.189	0.173
$C_{Lf}A$ [m²]	0.246	0.185
$C_{Lr}A$ [m²]	-0.057	-0.063
C_SA [m²]	-0.016	-0.026
$C_{Sf}A$ [m²]	-0.101	-0.110
$C_{Sr}A$ [m²]	0.116	0.136
M_xA [m²]	-0.058	-0.056

An increase in side-force can also be observed. Though many small modifications were made to the geometry, the modifications made to the windscreen and bellypan have the greatest effect. The extended, curved lower bellypan causes a high pressure region which provides a net side-force, aiding the rear tyre in producing cornering forces. The windscreen's increased size and modified curvature and height produce a low pressure area, which provides additional cornering forces to the front wheel. These two components thus show great promise as tools to improve motorcycle cornering performance through aerodynamics.

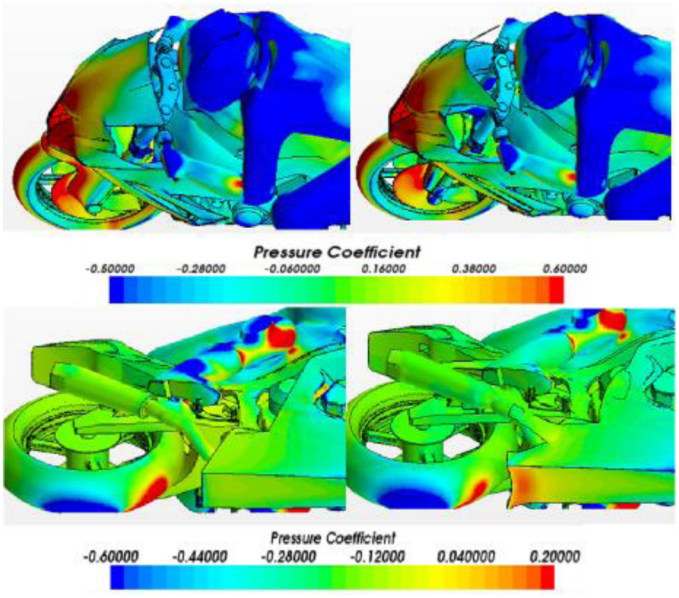

Figure 26. Pressure distribution (right view) showing side-force generated by belly pan and windscreen.

Summary

The flow around the motorcycle during a high-speed cornering manoeuvre from 45° to 55° of lean was simulated, and the full simulation set-up was discussed. A break-down of each orthogonal aerodynamic force's effect on performance is presented. The following conclusions can be made:

- The interaction of the high pressure field pushed in front of the vehicle with the ground is a primary cause of a substantial increase of lift and side-force under leaning conditions.
- Large moments are developed by the aerodynamic forces due to the motorcycle's orientation in lean. Their effect on contact patch lift and side-force is greater than that of the aerodynamic lift/side-force itself. Moments/tyre contact patch loads must therefore be considered when assessing motorcycle aerodynamic performance.
- Lift and drag force variation shows almost linear increase with increasing lean angle. Their effect on performance is therefore predictable.
- The side-force magnitude variation shows no pattern throughout the range of roll angles investigated, however its effect on performance is more consistent: yawing the vehicle out of the corner.
- Comparison of standard and modified parts at high lean angle shows promise for the use lower belly pan geometry to influence cornering performance. The drag optimised shape provided additional cornering forces to the rear tyre contact patch.
- Due to its orientation in lean, the windscreen has a large influence on both lift and side-force. A drag-optimised shape shows a reduction of its negative influences on these forces.

References

1. Bella, G., Krastev, V., Testa, M., and Leggio, E., "Application of an Integrated CFD Methodology for the Aerodynamic and Thermal Management Design of a Hi-Performance Motorcycle," SAE Technical Paper 2013-24-0143, 2013, doi:10.4271/2013-24-0143.
2. CD-Adapco. (2013) USER GUIDE STAR CCM+ Version 8.04.
3. Foale, Tony. *Motorcycle Handling and Chasis Design: The Art and Science*. Spain?: Tony Foale Designs, 2002.
4. Gullberg, P., Lofdahl, L., and Nilsson, P., "Cooling Airflow System Modeling in CFD Using Assumption of Stationary Flow," SAE Technical Paper 2011-01-2182, 2011, doi:10.4271/2011-01-2182.
5. Sakagawa, K., Yoshitake, H. and Ihara, E. "Computational Fluid Dynamics for Design of Motorcycle (Numerical Analysis of Coolant Flow and Aerodynamics)," SAE Technical Paper 2005-32-0033, 2005.
6. Saunders, J. and Mansour, R., "On-Road and Wind Tunnel Turbulence and its Measurement Using a Four-Hole Dynamic Probe Ahead of Several Cars," SAE Technical Paper 2000-01-0350, 2000, doi:10.4271/2000-01-0350.
7. Scappaticci, L., Risitano, G., Battistoni, M., and Grimaldi, C., "Drag Optimization of a Sport Motorbike," SAE Technical Paper 2012-01-1171, 2012, doi:10.4271/2012-01-1171.
8. Sedlak, V. (2012) "Motorcycle Cornering Improvement: An Aerodynamical Approach based on Flow Interference," MSc thesis. KTH Royal Institute of Technology.
9. Schütz, Thomas. *Hucho - Aerodynamik Des Automobils Strömungsmechanik, Wärmetechnik, Fahrdynamik, Komfort*. 6., Vollst. Überarb. U. Erw. Aufl. 2013. ed. Wiesbaden: Springer Vieweg, 2013.

10. Shimizu, T., Abe, T., Sunayama, Y., Watanabe, S., Nakamura, E. “Simultaneous Evaluation on Aerodynamics and Air-cooling Performances for Motorcycle using CFD Analysis,” SAE Technical Paper 2009-32-0138, 2009.
11. Takahashi, Y., Kurakawa, Y., Sugita, H., Ishima, T. and Obokata, T. “CFD Analysis of Airflow around the Rider of a Motorcycle for Rider Comfort Improvement,” SAE Technical Paper 2009-01-1155, 2009, doi:10.4271/2009-01-1155.
12. Yamaha Factory Racing “YZR-M1 Technical Presentation - The evolution of the YZR-M1 during the 990cc period”, Available at: http://mototribu.com/constructeur/yamaha/2006/r1/doc/2006%20YZR-M1%20Technical%20Presentation_tcm78-170625.pdf (Accessed 8 Sept 2014).

APPENDIX

APPENDIX A

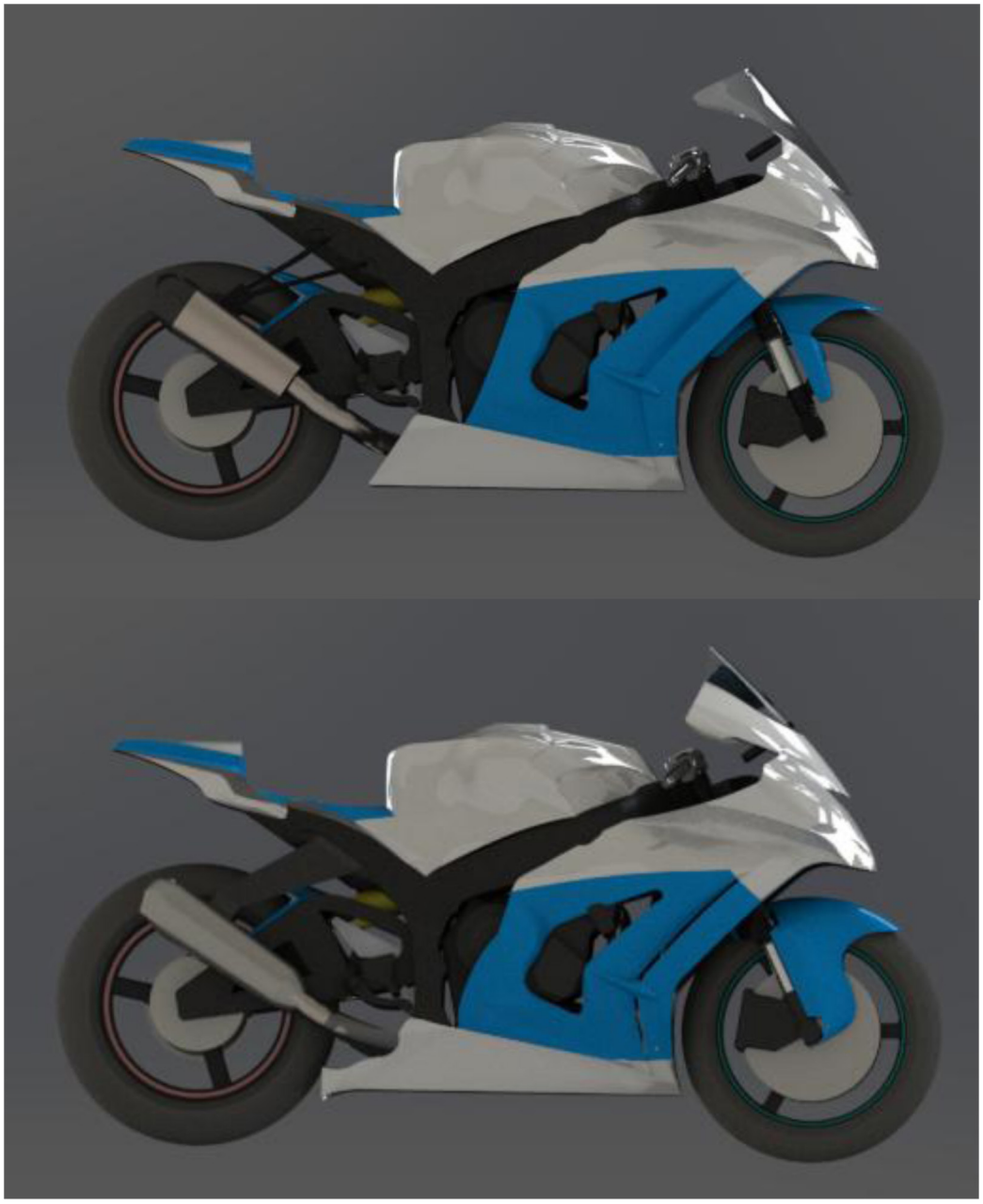

Figure 27. Comparison SuperStock (top) and SuperBike (bottom) for profile view.

The Engineering Meetings Board has approved this paper for publication. It has successfully completed SAE's peer review process under the supervision of the session organizer. The process requires a minimum of three (3) reviews by industry experts.

ISSN 0148-7191

http://papers.sae.org/2015-01-0097